

Research on gear fault diagnosis for nuclear power circulating water pump based on deep neural network

Zhibin Wei^{1,2}, Xintong Ma³, Zelin Nie^{1,2,*}, Zhao Xu³, Wei Cheng^{1,2}, Zhaoguo Wang^{1,2}, Zhuang Miao³, Li Li³, and Shuhong Du³

¹ School of Mechanical Engineering, Xi'an Jiaotong University, Xi'an 710049, PR China

² National Key Lab of Aerospace Power System and Plasma Technology, Xi'an Jiaotong University, Xi'an 710049, PR China

³ China Nuclear Power Engineering Co. Ltd., Beijing 100000, PR China

Received: 27 June 2025 / Accepted: 13 November 2025

Abstract. In nuclear power circulating water pump systems, gears, as critical transmission components, operate in low-speed, heavy-load environments and are crucial for maintaining the stable operation of the pump. To significantly enhance the efficiency and accuracy of fault diagnosis, this paper proposes a gear fault diagnosis technology based on deep neural networks. Efficient Fast Fourier Transform (FFT) techniques are employed to extract frequency domain samples containing rich fault information. Subsequently, a deep neural network model is designed and trained to automatically extract deep features from the frequency domain signals and accurately identify different fault types. By comparing the performance of various deep neural network models, precise diagnosis of gear faults in nuclear power circulating water pumps is achieved. This method is of significant importance for improving nuclear power safety, optimizing plant operational efficiency, and enhancing economic benefits.

Keywords: Nuclear power circulating water pump / Gear / Fault diagnosis / Deep neural network.

1 Introduction

Nuclear energy, as a renewable energy source, possesses the characteristic of being recyclable and reusable, and generates electricity through nuclear fission or nuclear fusion. Nuclear power not only has low carbon emissions and is environmentally friendly, but also operates with high stability and reliability. As an essential component of the global energy transition, nuclear energy will play a key role in achieving the goals of safety, reliability, and low-carbon environmental protection [1].

China attaches great importance to the research, development, and application of nuclear power unit condition monitoring and fault diagnosis technologies. From *The 12th Five-Year Plan for the Development of Science and Technology of the People's Republic of China* [2] to *Made in China 2025* [3], and then to the *Nuclear Safety in China* [4] white paper, the importance of strengthening research in the field of nuclear power equipment fault diagnosis has been clearly emphasized.

The circulating water system in nuclear power units provides cooling water to the three-loop condenser. The

circulating water pump drives the seawater circulation, delivering low-temperature seawater to the condenser to absorb heat, and then discharging the warmed seawater out of the system, carrying away the residual heat of the unit. The system schematic is shown in [Figure 1](#). The gear in the circulating water pump is a key rotating component responsible for low-speed, heavy-load transmission. If the single-side clearance of the gear exceeds the design specifications, it may not only cause friction between the impeller and the pump casing, damaging the circulating water pump, but it could also result in a significant power drop of up to 50%, causing an economic loss of approximately 10 million RMB per day for production [5]. Therefore, fault diagnosis of the gear is particularly critical to ensuring the safe and stable operation of the circulating water pump.

In recent years, relevant scholars have conducted extensive research on the characteristics of gear faults, where early degradation signals are weak and the consequences of failure are severe. Yang et al. used the wavelet packet decomposition algorithm to decompose the original vibration signals of rotating mechanical gears, constructed a feature set using the energy spectrum of the time-frequency information obtained, and input the feature set into a support vector machine for gear fault diagnosis in rotating

* e-mail: niezelin@xjtu.edu.cn

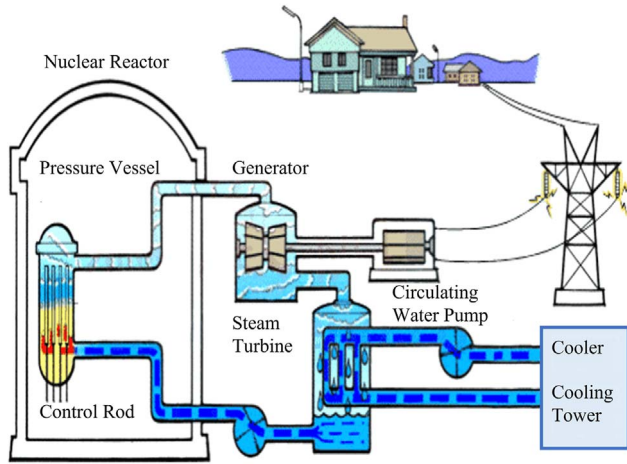


Fig. 1. Schematic diagram of nuclear power plant system.

machinery [6]. Amin et al. employed a Bayesian convolutional network to accurately diagnose gearbox faults in wind turbines and provide uncertainty estimates [7]. Wang et al. improved feature mode decomposition by combining Particle Swarm Optimization (PSO) and spectral Gini index to adaptively optimize key input parameters, effectively identifying weak fault features of planetary gearboxes under strong background noise and variable speed conditions [8]. Praveen et al. developed a multi-scale continuous wavelet algorithm that enables real-time detection of non-stationary load faults in the planetary gearbox of miniature wind turbines on a compact signal analyzer [9]. Calle et al. constructed a context-aware health indicator based on oil debris sensing and operating conditions, distinguishing damage severity and tracking its evolution [10]. Soualhi et al. proposed a method for early diagnosis of gear defects in gear reducers using a novel health indicator, which was validated under multiple load and variable speed conditions [11]. ThanhTung et al. assessed gear health by monitoring the magnetic coupling echo loss between the antenna and gear, and revealed the impact of coupling distance and phase fluctuation on echo characteristics under both static and high-speed conditions [12]. Vamsi et al. utilized the Hurst exponent of raw vibration and acoustic signals as a health indicator to diagnose faults in multi-stage gearboxes under variable speed operations [13]. Wan et al. developed a novel gearbox fault diagnosis method by integrating an optimized variational mode decomposition (VMD) and non-local means (NLM) filtering denoising technique with a one-dimensional deep residual shrinkage network [14]. Adel et al. proposed an intelligent algorithm for gear and bearing fault diagnosis, combining robust empirical mode decomposition, time-domain features, and an equilibrium optimizer [15]. Abdelrahman et al. introduced different ranking methods to select relevant features and employed data segmentation techniques to enhance the performance and scalability of predictive models. Through assessing the impact of data segmentation on gearbox predictive maintenance, they found that decision tree, SVM, and KNN models significantly

outperformed other models [16]. Shukla et al. addressed specific challenges in wind turbine gearboxes by utilizing a Bayesian convolutional neural network for fault diagnosis, providing precise results with uncertainty boundaries, and reducing misclassification errors [17].

Based on the aforementioned studies, the limitations of existing methods are mainly reflected in their weak ability to identify early faults in complex noise environments, reliance on manual expertise for feature extraction with poor robustness, and lack of adaptability in model parameter optimization. This paper proposes a method for gear fault identification by extracting frequency domain samples of failure features using Fast Fourier Transform (FFT), reducing the reliance on manual feature engineering, and designing a deep neural network model for gear fault recognition. Additionally, the PSO algorithm is introduced to enhance the efficiency and accuracy of the model's global search. Furthermore, the first experimental platform for nuclear power circulating water pump gear systems in China is established, providing an efficient and reliable solution for gearbox fault diagnosis in nuclear power circulating water pumps.

2 Theoretical methods

2.1 Theoretical framework of deep neural networks

In applications such as gear fault diagnosis, Deep Neural Networks (DNN) are capable of extracting fault features from complex signals, enabling fault diagnosis and prediction [18]. A DNN consists of three main components: The input layer, hidden layers, and output layer.

1) Input layer

The input data is a two-dimensional image of size $H \times W$ (height H , width W), which can be represented as an $H \times W$ matrix, with each element corresponding to a pixel in the image. This matrix is denoted as X , $X_{[i][j]}$ represents the value of the pixel located at the i -th row and j -th column of the image. The input layer serves as the entry point of the deep neural network, responsible for receiving and passing the raw data to the subsequent hidden layers for processing.

2) Hidden layer

The hidden layer consists of multiple neurons, each receiving the output from the previous layer as input. After being processed by an activation function, it generates an output. The output data of each neuron in the hidden layer is expressed by the following mathematical formula.

$$a = f\left(\sum_{i=1}^n w_i x_i + b\right).$$

Where a is the output of the neuron; f is the activation function; w_i is the connection weight; x_i is the input from the previous layer; b is the bias term; n is the number of neurons in the previous layer.

This formula describes how a neuron computes its output based on the input and weights.

3) Output layer

In gear fault diagnosis, the output layer is equipped with N neurons corresponding to the potential N fault types, with each neuron representing a specific fault type [19]. In classification tasks, the *SoftMax* activation function is commonly used in the output layer to ensure that the sum of the values of all output neurons equals 1, thereby reflecting the probabilities of different fault types. The calculation formula for the *SoftMax* activation function is:

$$P(y = j/x) = \frac{e^{z_j}}{\sum_{k=1}^K e^{z_k}}.$$

Where $P(y = j/x)$ is the probability of the output being the j th class given the input x ; z^j is the input value of the j th neuron in the output layer; K is the number of neurons in the output layer, which is also the number of fault types.

4) Inter-layer connections and weights

During the training process, the weight updates are calculated using the backpropagation algorithm to compute the gradients, which are then updated using optimization algorithms such as gradient descent. The goal of the weight update is to minimize the loss, enabling the network to better fit the training data and generalize to new data.

5) Activation function

The activation function not only introduces non-linearity to the network, enabling the neural network to approximate any functional relationship, but also enhances the model's generalization ability. By mapping the input data to a non-linear space, the activation function improves the network's learning capacity and adaptability [20].

2.2 Particle swarm optimization theory

To enable the model to accurately identify fault types, a new PSO algorithm is proposed. This algorithm is inspired by the intelligence and cooperation observed in the behavior of bird flocks. It is an optimization strategy based on swarm intelligence. Through this mechanism, the movement direction of the entire particle swarm becomes more organized, efficiently searching for and ultimately determining the optimal solution.

Algorithm structure:

1) Particle representation

In PSO, each candidate solution is considered a "particle". The particle adjusts its velocity and position based on its own historical best and the global best of the swarm, with the swarm collaboratively searching to approach the global optimum. When applied to neural networks, the position represents the weights or hyperparameters, and the fitness is typically measured by the accuracy of the validation set.

2) Fitness function

The fitness function determines the quality of particles. In gear fault diagnosis, it combines the false positive rate, false negative rate, with classification accuracy as the primary metric. The function rewards correct classifications

while penalizing false positives and false negatives, guiding the particles to improve precision and reduce errors, thus steering the search towards the optimal model.

3) Individual best and global best

In PSO, "individual best" and "global best" are two core concepts that guide the particle swarm in searching for the optimal solution.

To express mathematically, let the particle swarm consist of N particles, and the position of particle i in a D -dimensional space can be represented as:

$$X_i = (x_{\{1\}}, x_{\{2\}}, \dots, x_{\{D\}}).$$

Its velocity is:

$$V_i = (v_{\{1\}}, v_{\{2\}}, \dots, v_{\{D\}}).$$

The individual best position is denoted as:

$$pBest_i = (p_{\{1\}}, p_{\{2\}}, \dots, p_{\{D\}}).$$

Where $p_{\{ij\}}$ is the individual best position of particle i in the j th dimension.

The global best position is represented as:

$$gBest = (g_1, g_2, \dots, g_D).$$

Where g_j is the global best position of all particles in the j th dimension.

4) Velocity and position update

The core steps of the PSO algorithm are updating the velocity and position. The velocity update of a particle considers three main factors: The particle's current velocity, the influence of the particle's individual best position, and the influence of the global best position.

The velocity update formula is as follows:

$$v_i(t+1) = w \cdot v_i(t) + c_1 \cdot r_1 \cdot (pbest_i - x_i(t)) + c_2 \cdot r_2 \cdot (gbest - x_i(t)).$$

Where $v_{\{i\}}(t)$ is the velocity of particle i at time t ; w is the inertia weight, which adjusts the particle's reliance on its current velocity; c_1 and c_2 are the learning factors, which control the step size for the particle's learning towards its individual best and the global best, respectively; r_1 and r_2 are random numbers between $[0,1]$, which increase the diversity of the search; $(pbest_{\{i\}})$ is the individual best position of particle i ; $(gbest)$ is the global best position; $x_i(t)$ is the position of particle i at time t .

After updating the velocity, the particle calculates its next position based on the new velocity and current position.

The position update formula is relatively simple:

$$x_i(t+1) = x_i(t) + v_i(t+1).$$

Where $x_i(t+1)$ is the position of particle i at time $t+1$; $x_i(t)$ is the position of particle i at time t ; $v_i(t+1)$ is the velocity of particle i at time $t+1$.

By iteratively updating the velocity and position, the algorithm guides the particles to search in the direction of

the optimal solution, ultimately finding the best solution to the problem.

5) Iteration process

First, the number of particles N is determined, and initial positions and velocities are randomly assigned to the particles. The fitness function is then calculated, and each particle's individual best position (p_best) and the global best position (g_best) are recorded. The iteration begins: The velocity is updated based on the inertia weight w and learning factors c_1 and c_2 , followed by position update. If the particle exceeds the boundary, it is reflected back. The velocity update formula incorporates the inertia weight w , individual factor c_1 , and group factor, maintaining a balance between exploration and exploitation. The process continues until the stopping criteria are met, with the output being the optimal solution.

6) Termination condition

Stability of the solution quality: If the quality of the optimal solution shows no significant improvement or exhibits very little fluctuation, the algorithm can be terminated at this point.

The flow of the PSO algorithm is shown in Figure 2. Its termination condition is set based on the specific requirements of the problem and the algorithm's performance, aiming to ensure that the algorithm can find the optimal solution that meets the requirements within a reasonable time frame [21].

3 Model design

The fault diagnosis framework for circulating water pump gears based on Deep Neural Networks (DNN) is shown in Figure 3. In this framework, the frequency spectrum of mechanical vibration signals is first used as training samples and input into the network. Then, in the pre-training stage, the DNN automatically extracts fault features. Next, the fine-tuning process begins, where the output layer configuration is determined based on the mechanical health status, and the PSO algorithm is used to adjust the hyperparameters of the DNN. Finally, after the training is completed, the fault diagnosis results are outputted [21].

Each operating condition in the experimental dataset contains approximately twenty million data points. First, time-frequency domain analysis is used to preprocess the dataset, achieving data reduction and noise reduction. For a specific operating condition dataset, a rectangular window is applied to the time series signal, with a window size of six times the sampling frequency. The data is divided into 300 groups, and a FFT is performed on each group to obtain a one-dimensional frequency signal with a length of 2,048. At this point, the preprocessing of the dataset is completed, with 500 samples for each operating condition.

Before adjusting the parameters, the model structure is initially designed. The network consists of two fully connected layers and one *SoftMax* layer. The network parameters and connection order are shown in Table 1. The activation function selected is the non-linear, non-saturating ReLU function, which experiences a relatively fast gradient decay during the training phase.

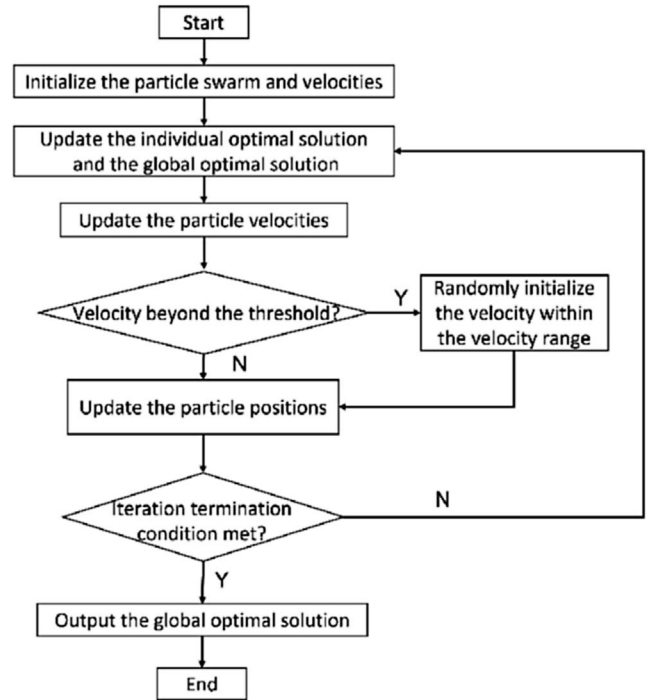


Fig. 2. PSO algorithm flow.

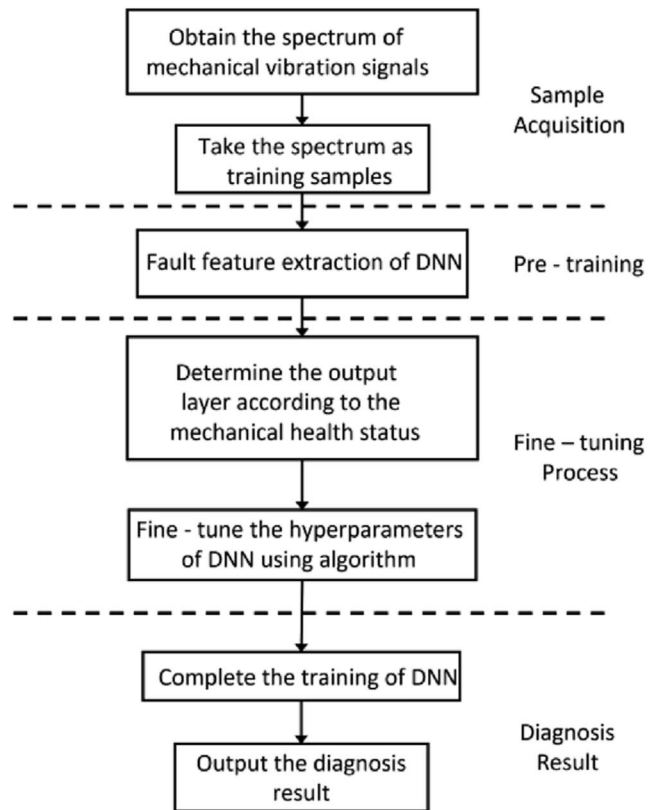


Fig. 3. Basic framework of the model.

Table 1. Model structure parameters.

Layer number	Layer name	Hyperparameters
1	Input layer	$2,048 \times 1$
2	Fully connected layer <i>ReLU</i> activation function	1,024
3	Fully connected layer <i>ReLU</i> activation function	248
4	SoftMax layer	4

In the network architecture diagram, the first layer is designed as the input layer, responsible for receiving the raw input data of size $2,048 \times 1$. The second layer is a fully connected layer containing 1,024 neurons. The third layer is also a fully connected layer, but the number of neurons is reduced to 248. After processing through the ReLU layer, the output consists of 248×1 computation results.

The fourth layer consists of 4 neurons, handling the classification problem of 4 operating states, with the SoftMax function used as the activation function.

4 Experimental study

4.1 Introduction to the experimental platform

Considering the limited reference value of public datasets for validating gear fault diagnosis methods, a collaborative effort was made with China National Nuclear Corporation, Shanghai Apollo Machinery Co., Ltd., and Xi'an Jiaotong University to develop the first domestic integrated experimental device focused on intelligent operation and maintenance research and technical validation for nuclear power circulating water pump gear drive systems, as shown in Figure 4. This circulating water pump has a body diameter of approximately 8 m, a height of 20 m, with a pump shaft speed of 183 revolutions per minute, and a motor power of up to 7,200 kW. To ensure the effectiveness of the test bench, the main structure and principles of the circulating water pump are consistent with the original product.

4.2 Typical gear fault types

Pre-faulted gears were experimentally tested, and data were collected. The physical representations of the pre-faulted gears are shown in Figure 5, which include four fault types: Healthy gear, tooth fracture, pitting, and spalling [22]. The experiment consists of 12 sets, categorized into four types: Healthy, tooth fracture, pitting, and spalling. Each type encompasses three operating conditions: Normal speed, high speed, and low speed. The sampling frequency is set at 10,240 Hz, with vibration signals recorded every 5 s [23]. Data for all four fault states were acquired. By analyzing and comparing the characteristic differences between healthy and faulty samples, a gear fault diagnosis model was developed.

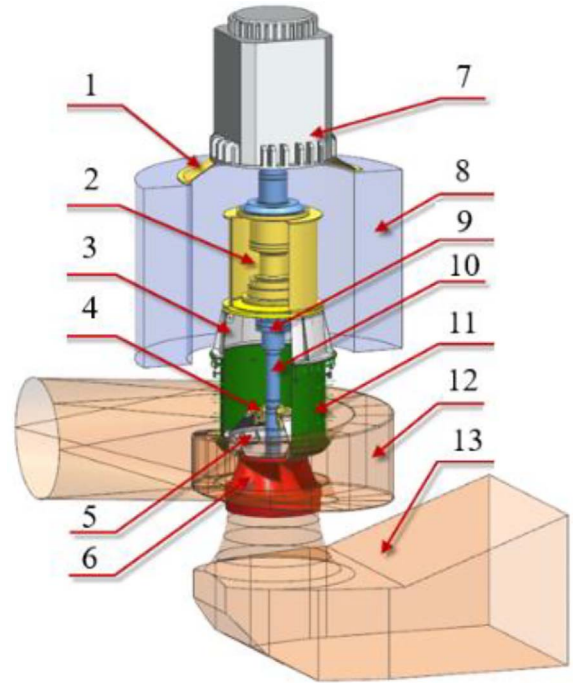


Fig. 4. Structural model of the experimental platform. The pump unit consists of: 1. Motor bracket, 2. Gearbox, 3. Gearbox bracket, 4. Guide bearing, 5. Pump cover, 6. Impeller, 7. Motor, 8. Concrete foundation, 9. Coupling, 10. Pump shaft, 11. Lining of the pit, 12. Volute casing, and 13. Inlet flow passage.



Fig. 5. (a) Healthy, (b) tooth fracture, (c) pitting, (d) spalling.

When analyzing the signal data of the gear fault dataset under rated operating conditions, both time-domain and frequency-domain signals provide key insights (Fig. 6). The complex operating environment of the gear and the vibration coupling between its components make fault diagnosis based solely on time-domain signals particularly challenging. Each operating condition sample consists of approximately 20 million sampling points, with a subset of 1,000 consecutive points selected for analysis.

In the healthy state, the amplitude of the gear's acceleration signal is approximately 0.8 m/s, with a smooth time-domain waveform, occasional minor fluctuations, and no significant periodic characteristics. When a tooth fracture

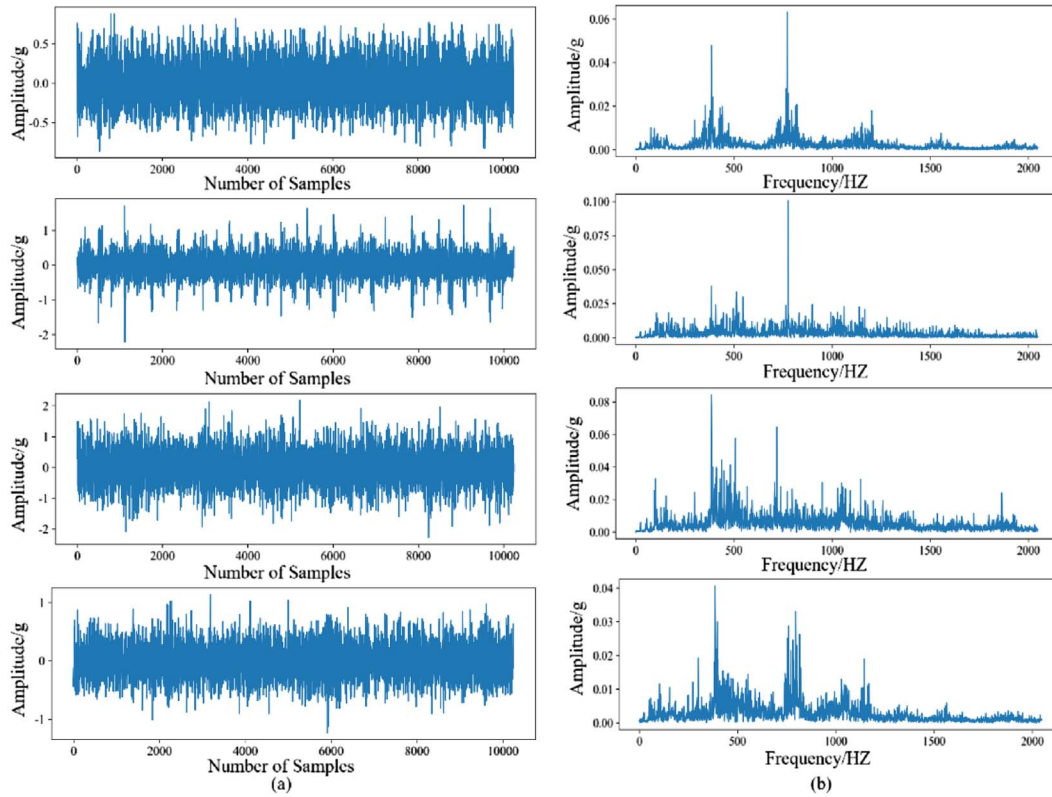


Fig. 6. (a) Time-domain signals of healthy, tooth fracture, pitting, and spalling gears. (b) Frequency-domain signals of healthy, tooth fracture, pitting, and spalling gears.

occurs, the acceleration signal amplitude increases to about 1.3 m/s, with noticeable abrupt changes and irregular fluctuations in the time-domain signal. In the pitting state, the gear's acceleration signal amplitude is approximately 2 m/s, and the time-domain waveform exhibits increased high-frequency noise and more abrupt changes. In the spalling state, the acceleration signal amplitude is about 1.1 m/s, with more frequent abrupt changes and irregular fluctuations in the time-domain signal.

For frequency-domain signal analysis, to accurately determine the gear fault type, the time-domain vibration signal is first transformed into a frequency-domain signal using FFT. In the healthy state, the gear exhibits a broad frequency distribution with relatively low amplitudes, with energy concentrated in the mid-to-low frequencies. In the case of tooth fracture, a significant peak appears at specific frequencies corresponding to the natural frequency of the broken area. For the pitting fault, there is a notable increase in high-frequency components, accompanied by multiple peaks, reflecting diverse vibration characteristics. In the spalling fault, low-frequency harmonics dominate with higher amplitudes, and the spectrum appears disordered, indicating strong interference with vibration characteristics. These frequency-domain differences provide essential insights for gear fault diagnosis.

In conclusion, relying solely on the amplitude and periodic characteristics of time-domain signals makes it difficult to distinguish between different gear fault types. To

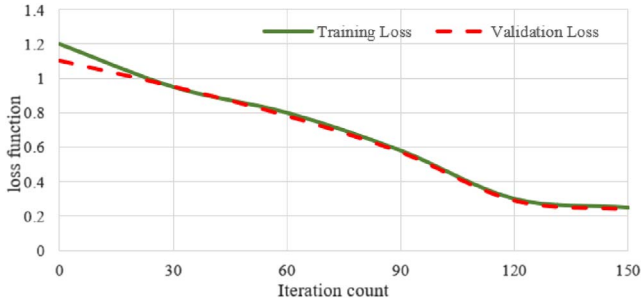
improve the accuracy and reliability of gear fault diagnosis, we recommend analyzing both time-domain and frequency-domain signal features. Time-domain signals provide information on instantaneous changes, while frequency-domain signals help identify more stable fault characteristics. Moreover, noise signals impede accurate fault identification. To enhance the accuracy and reliability of gear fault diagnosis, considering both time-domain and frequency-domain signal characteristics in tandem can significantly improve the efficiency and precision of fault diagnosis.

4.3 Neural network experimental validation

To evaluate the effectiveness of the algorithm, the deep neural network model was tested and analyzed using the circulating water pump gear fault dataset [24]. The sample division is shown in Table 2, which ensure the rigor and reproducibility of the study. Four types from the dataset were selected: Gear pitting, gear spalling, tooth fracture, and healthy gears, with each type containing 500 input samples. 10% of the total samples, i.e., 200 samples, were used as the test set, while the remaining samples were divided into training and validation sets in a 7:2 ratio. The training set contains 1,400 samples, and the validation set contains 400 samples. Among them, the uneven sampling better reflects the actual failure scenarios of the gear in the nuclear power plant circulating water pump. The load was set to the rated load for all samples.

Table 2. Experimental dataset division.

Damage type	Healthy	Broken tooth	Pitting	Spalling
Label	1	2	3	4
Training	350	350	350	350
Validation	96	98	101	105
Testing	50	50	50	50

**Fig. 7.** Model convergence curve.

After selecting the hyperparameters, the loss function of the model is shown in Figure 7.

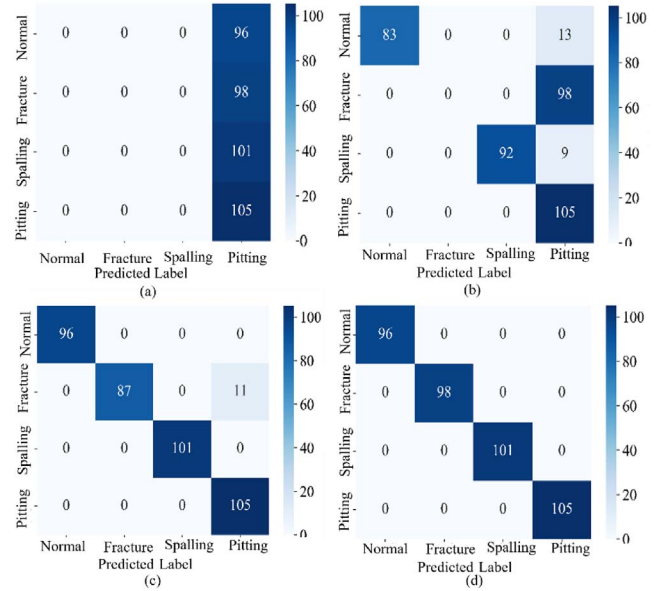
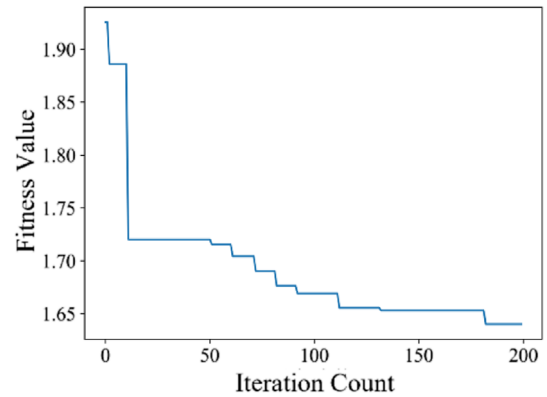
The figure contains two curves: The green curve represents the loss on the training set, while the red curve represents the loss on the validation set. At approximately 30 iterations, the two curves intersect, after which the validation set loss curve gradually decreases, indicating that the model's prediction accuracy on the validation set is improving. Meanwhile, the training set loss curve also decreases slowly showing that the model has converged after training. Both the training loss and validation loss show a downward trend and eventually stabilize, indicating that the model effectively converges during the training process.

As the number of iterations increases, the model's classification performance improves, and the misclassification rate decreases, as shown in Figure 8. However, this method requires a relatively high number of iterations, resulting in longer computation times. Therefore, the PSO algorithm is introduced to optimize the model's hyperparameters.

The initialization parameters for the PSO are set as follows: Swarm size $N = 50$, particle dimension $D = 2$, iteration count $k = 200$, inertia weight $\omega = 0.5$, and both individual and global learning factors are set to $G = 0.5$.

As shown in Figure 9, during the initial phase of iterations (from iteration 0 to 50), the function value sharply decreases from approximately 1.95. As the number of iterations increases (from 50 to 200), the function value gradually decreases and ultimately stabilizes around 1.65. After several iterations, the function value reaches stability, indicating that the algorithm has found the optimal solution. The results of the PSO algorithm hyperparameter optimization are as follows: The number of neurons is 941 and 1,915, and the learning rate is 0.0997.

During the training process, the training set loss exhibits an inverse relationship with the number of iterations. Initially, the training set loss is as high as 0.8, but it

**Fig. 8.** Model classification results after iterations. (a) 10 iterations, (b) 20 iterations, (c) 30 iterations, (d) 40 iterations.**Fig. 9.** PSO algorithm convergence curve.

gradually decreases as the number of iterations increases. At iteration 5, the loss drops to near zero and remains stable. In contrast to the training set loss, the validation set loss remains relatively stable and is generally smaller in magnitude. The validation set loss is used to evaluate the model's performance on new data. In Figure 10a, the validation set loss starts at approximately 0.6, and decreases as the number of iterations increases, although the reduction is relatively small, with minimal fluctuation. The model reaches convergence after the training process. In Figure 10b, after introducing the PSO algorithm, better classification results can be achieved with fewer iterations.

5 Conclusion

In the field of operational maintenance for nuclear power circulating water pump gears, this paper focuses on the issue of fault diagnosis. By constructing a fault

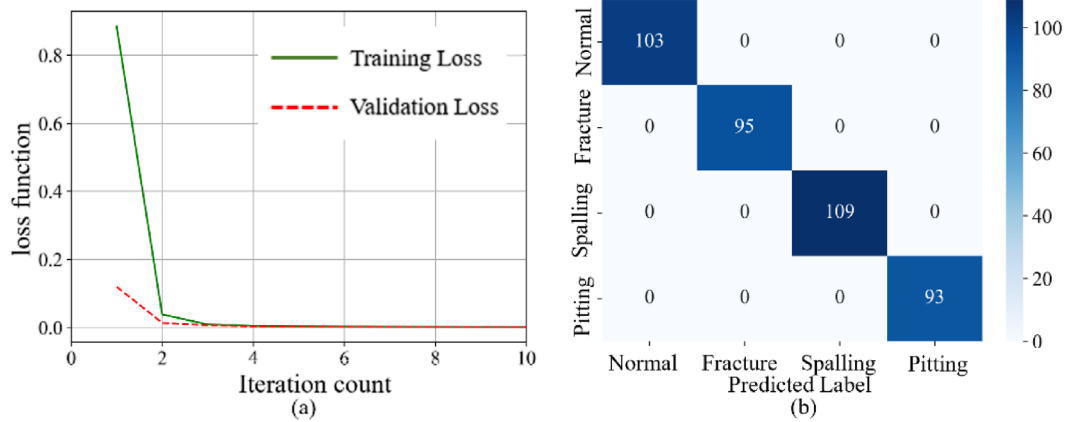


Fig. 10. (a) Model convergence curve after introducing the PSO algorithm. (b) Model classification results after introducing the PSO algorithm.

diagnosis model incorporating the PSO algorithm, the study effectively combines theory with practice, offering an in-depth exploration of the gear operation and maintenance strategy.

(1) Addressing the issue of data collection difficulties in the operational maintenance of nuclear power circulating water pump gears, Xi'an Jiaotong University, in collaboration with industry, has established the first domestic experimental platform for circulating water pump gears, compensating for the lack of operational maintenance data. The analysis shows that gear faults are correlated with vibration acceleration. Although there are small differences in the time domain, the amplitude distribution differences in the frequency domain are significant.

(2) Through effective data preprocessing techniques and an optimized model mechanism, an efficient and stable fault diagnosis model was developed. Experimental results indicate that this model not only demonstrates excellent accuracy and stability but also improves its performance by incorporating the PSO algorithm. The PSO algorithm, with its unique advantages, broad applicability, simple parameter setup, rapid convergence to the optimal solution, and strong global search and high adaptability, has exhibited outstanding performance in optimization problems, providing robust support for the model's optimization.

Funding

This work was supported by the National Natural Science Foundation of China (No. 52305130), the National Key Research and Development Program of China under Grant 2024YFB3310703, the Innovative Scientific Program of China National Nuclear Corporation (CNNC), and the support of K. C. Wong Education Foundation.

Conflicts of interest

The authors have nothing to disclose.

Data availability statement

Data associated with this article cannot be disclosed due to legal/ethical/other reason.

Author contribution statement

Conceptualization, Z. N.; Methodology, Z. W.; Software, Z.W.; Validation, Z. W.; Formal Analysis, Z. N.; Investigation, Z.W.; Resources, X. M., Z. X., Z. M., L. L., S. D.; Curation, W. C.; Writing – Original Draft Preparation, Z.W.; Writing – Review & Editing, Z. N.; Visualization, Z.W.; Supervision, W.C.; Project Administration, W.C.; Funding Acquisition, W.C.

References

- 1 Y. Shu, et al., Building a new electric power system based on new energy sources, *Strateg. Study Chin. Acad. Eng.* **23**, 61–69 (2021).
- 2 S. Ling, China's neighborhood security cooperation under the holistic approach to national security, *J. Int. Secur. Stud.* **42**, 28–52, 156, 157 (2024).
- 3 G. Chai, et al., Nuclear safety improvement actions and safety requirements in post-Fukushima era, *Atom. Energy Sci. Technol.* **56**, 399–409 (2022).
- 4 C. Zhao, Development status and outlook for nuclear power in China, *Nucl. Power Eng.* **3**, 13 (2018).
- 5 X. Liang, J. Zuo, Z. Feng, Dynamic modeling of gearbox faults: A review, *Mech. Syst. Signal Process.* **98**, 852–876 (2018).
- 6 X. Yang, et al., A new fault diagnosis method for multistage gearbox based on GAPSO-SVM, *J. Xi'an Univ. Technol.* **38**, 519–525 (2022).
- 7 A. Amin, et al., A Bayesian deep learning framework for reliable fault diagnosis in wind turbine gearboxes under various operating conditions, *Wind Eng.* **48**, 297–309 (2024).
- 8 C. Wang, et al., Weak fault diagnosis of planetary gearbox based on IFMD under time-varying speed, *J of Vib. Eng.* **37**, 1980–1992 (2024).
- 9 M. Praveen, et al., Wavelet based real-time planetary gearbox health monitoring under non-stationary operation, *Exp. Tech.* **46**, 861–875 (2022).
- 10 D. Calle, et al., A context-aware oil debris-based health indicator for wind turbine gearbox condition monitoring, *Energies.* **12**, 33–73 (2019).
- 11 M. Soualhi, et al., Health monitoring of bearing and gear faults by using a new health indicator extracted from current signals, *Measurement* **141**, 37–51 (2019).

- 12 M. ThanhTung, et al., Effect of phase fluctuation on the proper operation of smart gear health monitoring system, *Sensors* **22**, 3231(2022).
- 13 I. Vamsi, et al., An integrated condition monitoring scheme for health state identification of a multi-stage gearbox through Hurst exponent estimates, *Struct. Health Mon.* **22**, 730–745 (2023).
- 14 Z. Wan, et al., Gearbox fault diagnosis method based on optimized VMD-NLM with 1DDRSN, *J. Mech. Transm.* **49**, 150–160 (2025).
- 15 A. Adel, et al., Gearbox fault diagnosis using REMD, EO and machine learning classifiers, *J. Vib. Eng. Technol.* **12**, 4673–4697 (2023).
- 16 A. Abdelrahman, et al., Vibration based fault diagnostics in a wind turbine planetary gearbox using machine learning, *Wind Eng.* **47**, 175–189 (2023).
- 17 K. Shukla, et al., Enhancing gearbox fault diagnosis through advanced feature engineering and data segmentation techniques, *Machines.* **12**, 261 (2024).
- 18 J. Ding, D. Xiao, X. Li, Gear Fault Diagnosis based on genetic mutation particle swarm optimization VMD and probabilistic neural network algorithm, *IEEE Access.* **8**, 18456–18474 (2020).
- 19 F. Wang, H. Gong, Q. Ni, Non-intrusion gear fault diagnosis of 400 km/h+ high-speed train based on signal fusion of stator current and electromagnetic torque, *Int. J. Automot. Technol.* **113** (2025).
- 20 F. Liu, et al., Spectral denoising random feature decomposition and its application in gear fault diagnosis, *Appl. Acoust.* **231**, 110562 (2025).
- 21 P. Goswami, N. Rai, A Novel methodology for chipped teeth and worn tooth gear fault detection using minimum entropy deconvolution and CEEMDAN, *J. Vib. Eng. Technol.* **13**, 11 (2025).
- 22 M. Batsch, B. Kiczek, Gear fault detection method based on convex hull clustering of autoencoder’s latent space, *Appl. Sci.* **14**, 5282 (2024).
- 23 H. Wang, et al., Fault diagnosis of planetary gearbox using ICEEMDAN and SVM, *Mech. Sci. Technol. Aerosp. Eng.* **42**, 24–30 (2023).
- 24 J. Zheng, H. Pan, Mean-optimized mode decomposition: An improved EMD approach for non-stationary signal processing, *ISA Trans.* **106**, 392–401 (2020).

Cite this article as: Wei Z, Ma X, Nie Z, Xu Z, Cheng W, et al. Research on gear fault diagnosis for nuclear power circulating water pump based on deep neural network, *Res. Des. Nucl. Eng.* **2**, 2025010 (2026), <https://doi.org/10.1051/rdne/2025010>.